

Structural, optical, and electrical properties of bulk single crystals of $\text{InAs}_x\text{Sb}_{(1-x)}$ grown by rotatory Bridgman method

V. K. Dixit,^{a)} Bhavtosh Bansal, V. Venkataraman, and H. L. Bhat^{b)}
Department of Physics, Indian Institute of Science, Bangalore 560012, India

G. N. Subbanna
Materials Research Centre, Indian Institute of Science, Bangalore 560012, India

Radially-homogeneous and single-phase $\text{InAs}_x\text{Sb}_{(1-x)}$ crystals, up to 5.0 at. % As concentration, have been grown using the rotatory Bridgman method. Single crystallinity has been confirmed by x-ray and electron diffraction studies. Infrared transmission spectra show a continuous decrease in optical energy gap with the increase of arsenic content in InSb. The measured values of mobility and carrier density at room temperature (for $x=0.05$) are $5.6 \times 10^4 \text{ cm}^2/\text{V s}$ and $2.04 \times 10^{16} \text{ cm}^{-3}$, respectively.

InSb has the smallest energy gap (0.17 eV) among the binary III-V semiconductors. Although the energy gap of InAs (0.38 eV) is larger by 0.21 eV, a substantial bowing in the energy gap to values below that of InSb occurs when a small amount of arsenic replaces antimony. The energy gap of $\text{InAs}_x\text{Sb}_{(1-x)}$ continuously decreases with increasing x and attains a minimum value of 0.1 eV for $x=0.4$,¹⁻³ at room temperature. Hence this material is useful for room temperature infrared detectors operating in the 8–12 μm wavelength range.³⁻⁵ Furthermore, the very low effective mass of $\text{InAs}_x\text{Sb}_{(1-x)}$ across the compositional range⁶ raises the prospect of using this material for various galvanomagnetic applications. Although the benefits of alloying As in InSb had been discovered and studied for more than 30 years now, all studies carried out on bulk samples have been on crudely prepared polycrystals.^{2,7,8} There has been no report on the growth and properties of $\text{InAs}_x\text{Sb}_{(1-x)}$ bulk single crystals for any value of x . On the other hand by employing nonequilibrium techniques like molecular beam epitaxy,⁴ melt epitaxy^{9,10} and metalorganic chemical vapor deposition,⁵ epitaxial films of this material have been grown. Recent works on $\text{InAs}_x\text{Sb}_{(1-x)}$ are also on thin films and superlattice structures.^{11,12} In this letter, we report on growth and salient features from structural, optical, and electrical studies on bulk single crystals of $\text{InAs}_x\text{Sb}_{(1-x)}$, for $0 < x < .05$. These crystals were grown using the rotatory Bridgman method.¹³

$\text{InAs}_x\text{Sb}_{(1-x)}$ was synthesized by diffusing arsenic into high purity InSb. The starting material was taken in five different molar proportions viz., InSb:As::95:5, 90:10, 85:15, 80:20, and 75:25. The phase diagram of In–As–Sb has been well studied both theoretically and experimentally,^{14,15} from which the initial reaction temperatures were determined to be in the range of 600 to 700 °C for various compositions. It was found that homogeneous single crystals of $\text{InAs}_x\text{Sb}_{(1-x)}$ could be grown only up to starting proportions of 90:10,

beyond which the grown crystals were inhomogeneous and often phase separated. Consequently results are discussed only for the growth runs carried out with InSb:As ratios of up to 90:10. The starting materials were cleaned, degreased, and filled in an ampoule made from semiconductor grade (GE 214) quartz tube of 8 mm inner diameter. The ampoule was evacuated to 10^{-6} Torr and then sealed by fusing. The ampoule was given a 28° conical taper to initiate good seeding. To promote synthesis, the sealed ampoule was placed in the suitable temperature zone of the furnace in the rotatory Bridgman setup.¹³ Figure 1 shows the furnace temperature profile and the position of the ampoule with respect to it. The growth setup was inclined at an angle of 22° from the horizontal to ensure the initial seeding at the ampoule tip. For growth, temperature of the furnace was increased to 625 °C which is the melting point of antimony and well above the sublimation temperature of arsenic. At this point, to have a proper mixing between melt and As vapor, the ampoule was rotated in reverse. It may be pointed out that at 625 °C the vapor pressure of arsenic is over 1 bar, and hence heating the ampoule above this temperature often led to ampoule cracking. The reason for heating the ampoule well above the sublimation temperature is to thermally assist the diffusion process, which enhances the incorporation of arsenic in InSb. The accelerated crucible rotation¹³ (60 rpm peak rotation), coupled with the ampoule inclination, ensures InSb melt motion in radial and axial directions. The diffusion of arsenic

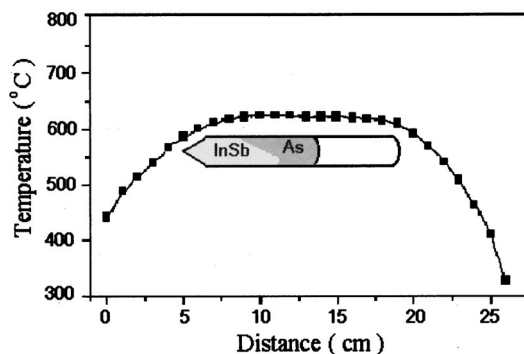


FIG. 1. Temperature profile and the position of the ampoule in the furnace.

^{a)}Present address: R & D Block “A,” Laser Physics Division, Centre for Advanced Technology, Indore-452013, M.P., India

^{b)}Author to whom correspondence should be addressed; electronic mail: hlbhat@physics.iisc.ernet.in

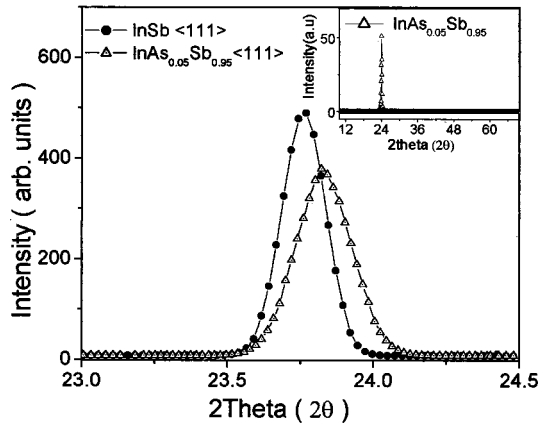


FIG. 2. X-ray diffraction peaks of InSb and InAs_{0.05}Sb_{0.95} wafers. The inset shows an x-ray diffraction pattern of InAs_{0.05}Sb_{0.95} wafer for 2θ scan from 10° to 70° .

vapor from the high to low temperature side through the melt was further facilitated by these rotation cycles. After 6 h of mixing, the growth was initiated by moving the furnace along the ampoule axis with a traverse rate of 8 mm/h. It may be pointed out that though the ampoule is tilted by 22° from the horizontal, the liquid solid interface is not parallel to the horizontal during growth. This is essentially because the accelerated crucible rotation was imposed on the ampoule. It was experimentally observed that the liquid–solid interface was slightly concave and symmetric with respect to ampoule axis. Typical size of the grown crystals were 8 mm diameter and about 45 mm length. The ingots were single crystalline upto ≈ 35 mm after which they were of multi-grain. Wafers were made from the 10–20 mm region from the tip of the ingot.

The melting point of InAs_xSb_(1-x) crystals as found by differential scanning calorimetry (DSC) was 570°C . This indicates that As concentration (inferred from the phase diagram of InAs_xSb_(1-x)¹⁵) must be more than 3 at. %. Presence of a sharp single endothermic peak in the DSC graph indicates the absence of any secondary phase. The composition x in InAs_xSb_(1-x) crystals grown from starting proportions of 95:5 and 90:10 were .02 and .05, respectively, as determined from energy dispersive x-ray analysis. The grown crystals were radially homogeneous, but the As composition decreased from tip to the other end of the ingot.

A single x-ray diffraction (XRD) peak (at $2\theta = 23.86^\circ$) for InAs_{0.05}Sb_{0.95} wafer confirms (111) orientation of the ingot (inset in Fig. 2). The XRD peak for the (111) reflection showed a clear shift towards higher angle relative to that of InSb, indicating a lattice contraction due to As substitution (Fig. 2). The lattice parameters of InSb and InAs_{0.05}Sb_{0.95}, as calculated from XRD, were $6.4782 \pm .0006$ and $6.4606 \pm .0006$ Å respectively and reasonably match the values obtained from Vegard's law. The bright field transmission electron microscope (TEM) image of a InAs_{0.05}Sb_{0.95} sample is shown in Fig. 3(a). Its selected area electron diffraction pattern [Fig. 3(b)] confirms zinc blende structure and absence of any twinning. However in the bright field image dislocations were observed which are primarily along the $\langle 110 \rangle$ direction [Fig. 3(c)]. The estimated dislocation density was $\approx 10^8 \text{ cm}^{-2}$. This is comparable to those found for InAs_xSb_(1-x) alloy grown by various other techniques.¹⁶

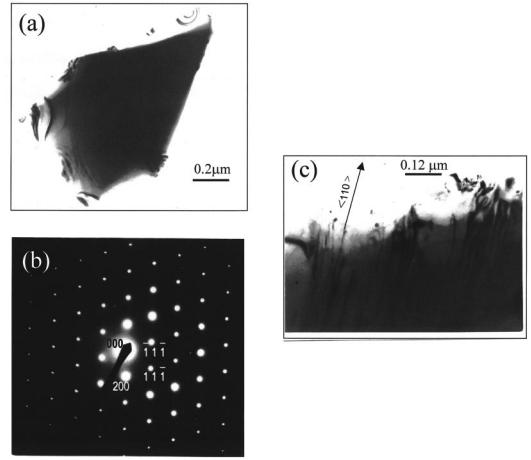


FIG. 3. (a) Bright field image of InAs_{0.05}Sb_{0.95}. (b) Selected area diffraction pattern of (a). (c) Bright field image showing dislocations along the $\langle 110 \rangle$ direction.

The Fourier transform infrared (FTIR) transmission spectra recorded for InAs_xSb_(1-x) ($x=0.02, 0.05$) wafers in the wavelength range of 3–25 μm are shown in Fig. 4. An IR spectrum of InSb is included in this figure for comparison. The IR spectra of both the InAs_xSb_(1-x) samples show a shift of absorption edge to lower energy. The room temperature energy gaps for the three samples, calculated using the relation $\alpha \sim (E_g - h\nu)^{1/2}$, were measured to be 0.17, 0.16, and 0.15 eV for $x=0, 0.02$, and 0.05 , respectively.

Resistivity and low field (< 0.2 T) Hall coefficient for five InAs_xSb_(1-x) samples with $x=0.02$ (three samples) and $x=0.05$ (two samples) were measured between 12 to 300 K. The RT mobility in the samples for $x=.02$ was $4.5 \times 10^4 \text{ cm}^2/\text{V s}$, and for $x=.05$ was $5.6 \times 10^4 \text{ cm}^2/\text{V s}$. All samples with $x=0.02$ were n -type and showed an intrinsic behavior above ≈ 250 K. The representative results for $x=0.02$ samples, shown in Fig. 5, give a RT carrier concentration of $6.4 \times 10^{16}/\text{cm}^3$, and a background doping of $5 \times 10^{16}/\text{cm}^3$, determined from the value of Hall coefficient measured at 15 K. The mobility peaks at around 250 K, after which it begins to fall, limited by a combination of electron, hole, and phonon scattering.¹⁷ The values obtained show that alloy scattering is not important in limiting the mobility. It is the large dislocation density (as evaluated from the TEM

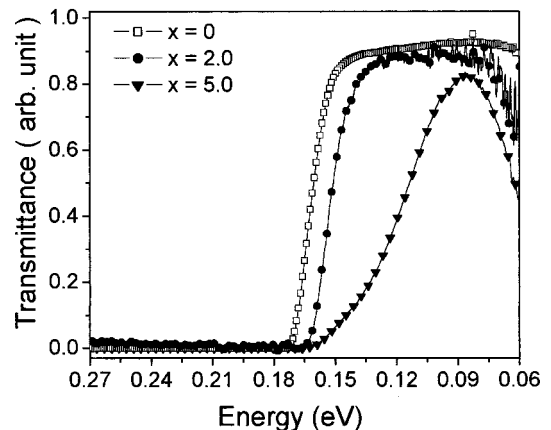


FIG. 4. RT infrared spectra of bulk InSb (for comparison) and InAs_xSb_(1-x).

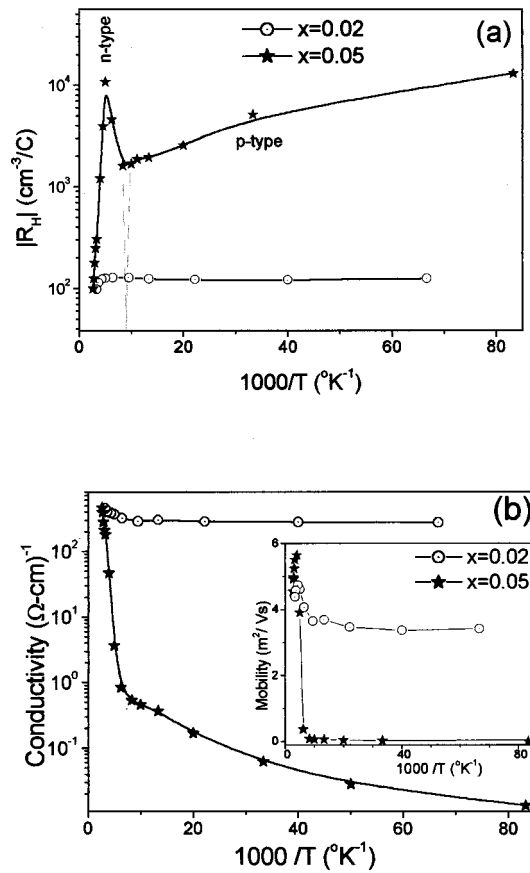


FIG. 5. Temperature dependence of (a) Hall coefficient, and (b) conductivity and mobility (inset) of $\text{InAs}_x\text{Sb}_{(1-x)}$.

images), that strongly affects the mobility, especially at low temperatures. The values and the temperature dependence of mobility below 200 K were seen to vary considerably between different samples, being particularly sensitive to number, charge, and the nature of dislocations present. For the sample reported, the mobility at 15 K was $3.37 \times 10^4 \text{ cm}^2/\text{Vs}$. The sample with $x=0.05$ shows a type conversion from n to p at 110 K. The carrier concentration measured at RT was $2.04 \times 10^{16}/\text{cm}^3$, in agreement with the calculated value of the intrinsic carrier concentration.⁶ Below 77 K, the Hall coefficient and resistivity did not saturate and the conductivity below 30 K was strongly activated, indicating the presence of acceptor-like trap states. Further evidence

of their presence is given by the pronounced tail in the absorption edge¹⁸ for this sample (Fig. 4). The hole mobility continuously dropped with a decrease in temperature to $175 \text{ cm}^2/\text{Vs}$ at 15 K.

In conclusion, we have grown radially homogeneous and single phase $\text{InAs}_x\text{Sb}_{(1-x)}$ crystals, up to 5 at. % As concentration using the rotatory Bridgman method. XRD and TEM studies reveal their single crystalline nature and a compressed lattice as compared to InSb. FTIR transmission spectra taken at RT, show a continuous shift in energy gap with increasing arsenic concentration. For $x=0.05$ the measured values of mobility and carrier density at RT were $5.6 \times 10^4 \text{ cm}^2/\text{Vs}$ and $2.04 \times 10^{16} \text{ cm}^{-3}$, respectively. The RT cutoff wavelength at $8.3 \mu\text{m}$ along with the high mobility and low background doping should make these single crystals useful in developing long wavelength infrared detector.

This work is partially supported by a DTSR project which is gratefully acknowledged. One of the authors (V. K. D.) acknowledges CSIR, India, for the award of a senior research fellowship.

- ¹J. C. Woolley and J. Warner, *Can. J. Phys.* **42**, 1879 (1964).
- ²W. M. Coderre and J. C. Woolley, *Can. J. Phys.* **46**, 1207 (1968).
- ³C. E. A. Grigorescu and R. A. Stradling, *Handbook of Thinfilm Devices* edited by M. H. Francombe (Academic, New York, 2000), Vol. 2, p. 27.
- ⁴M. Y. Yen, B. F. Levine, C. G. Bethea, K. K. Choi, and A. Y. Cho, *Appl. Phys. Lett.* **50**, 927 (1987).
- ⁵J. D. Kim, D. Wu, J. Wojtkowski, J. Piotrowski, J. Xu, and M. Razeghi, *Appl. Phys. Lett.* **68**, 99 (1996).
- ⁶A. Rogalski and K. Jozwikowski, *Infrared Phys.* **29**, 35 (1989).
- ⁷I. Kudman and L. Ekstrom, *J. Appl. Phys.* **39**, 3385 (1968).
- ⁸J. C. Woolley and J. Warner, *J. Electrochem. Soc.* **111**, 1142 (1964).
- ⁹Y. Z. Gao, H. Kan, M. Aoyama, and T. Yamaguchi, *Jpn. J. Appl. Phys.* **39**, 2520 (2000).
- ¹⁰Y. Z. Gao, H. Kan, F. S. Gao, X. Y. Gong, and T. Yamaguchi, *J. Cryst. Growth* **234**, 85 (2002).
- ¹¹D. Wu, B. Lane, H. Mohseni, J. Diaz, and M. Razeghi, *Appl. Phys. Lett.* **74**, 1194 (1999).
- ¹²B. Lane, Z. Wu, A. Stein, J. Diaz, and M. Razeghi, *Appl. Phys. Lett.* **74**, 3438 (1999).
- ¹³V. K. Dixit, B. V. Rodrigues, and H. L. Bhat, *J. Cryst. Growth* **217**, 40 (2000).
- ¹⁴P. S. Dutta and T. R. Miller, *J. Electron. Mater.* **29**, 956 (2000).
- ¹⁵C. H. Shih and E. A. Peretti, *Trans. Am. Soc. Met.* **48**, 708 (1956).
- ¹⁶R. J. Egan, V. W. L. Chin, and T. L. Tansley, *J. Appl. Phys.* **75**, 2473 (1994).
- ¹⁷V. W. L. Chin, R. J. Egan, and T. L. Tansley, *J. Appl. Phys.* **69**, 3571 (1991).
- ¹⁸G. R. Allan, H. A. Mackenzie, J. J. Hunter, and B. S. Wherrett, *Phys. Status Solidi B* **149**, 383 (1988).